Measurements of ultra-high energy lead ions using silicon and diamond detectors

Carlo Cazzaniga [a],[*], Maria Kastriotou [a], Rubén García Alía [b], Pablo Fernandez-Martinez [b], Vanessa Wyrwoll [b], Triestino Minniti [c], Christopher D. Frost [a]

[a] *ISIS Facility, UKRI-STFC, Rutherford Appleton Laboratory, Didcot OX11 0QX, UK*
[b] *CERN, CH-1211, Genève, Switzerland*
[c] *UKAEA, Culham Centre for Fusion, Energy, OX14 3DB, UK*

ARTICLE INFO

ABSTRACT

A silicon detector and a diamond detector have been used at the SPS experimental North Area at CERN for diagnostics of beams of ultra-high energy lead ions (150 GeV/nucleon).

The detectors are operated in pulse mode using a fast digital electronic chain. The discrimination capability of the two detectors is investigated using deposited energy and pulse shape analysis. It is shown that the detectors have good beam monitoring performances and can discriminate the main lead ion beam component from contamination of light and heavy fragments.

1. Introduction

The Super Proton Synchrotron (SPS), measuring nearly 7 kilometres in circumference, is the second-largest accelerator of the CERN accelerator complex [1]. It usually operates with protons up to 450 GeV, but it can also accelerate heavy ions during the dedicated CERN ion physics runs [2]. The SPS accelerator's main purpose is to feed the ions to the Large Hadron Collider (LHC), where collisions are exploited for high energy physics experiments. At the same time the SPS accelerator can deliver the high energy ions to other experimental areas, like the SPS North Area (SPS-NA) [3]. Here one of the applications of the ultra-high energy ions is the study of single event effects on microelectronics [4].

Ion beams are routinely used to test Single Event Effects (SEE) in microelectronics [5], in particular for space and accelerator applications [6–9], where the electronics needs to operate in elevated radiation fields with a high level of reliability. Most of the testing worldwide is performed at lower energies, typically between 10 and 100 MeV per nucleon. The SPS accelerator at CERN is a unique facility in terms of the available ultra-high energy range that it can access (hundreds of GeV per nucleon). The main reason for the exploitation of these energies is that test engineers can study the effect of relatively high Linear Energy Transfer (LET) combined with a beam that at the same time is highly penetrating. This fact allows for multiple boards to be stacked one after the other and tested in parallel with a moderate beam attenuation [10]. Also, ions maintain a constant LET throughout the entire sensitive volume of the component, which is easier for the data analysis of SEE. Furthermore, there is no need to remove the lids and housing of the microchip, operations that can be particularly difficult

if not impossible on systems that are highly compact and integrated, or with 3D structures.

It is clear that a beam with such high energy poses challenges in terms of accurate dosimetry, in particular for the measurement of the contamination by fragments (neutrons, protons or other ions) that can be generated by the interaction of the primary beam with the beam intercepting devices, such as collimators and beam instrumentation, and the Devices Under Test (DUTs).

In this work, the use of silicon and diamond detectors is studied. The main advantage of these solid state detectors is the small dimensions (2×2 mm^2) that allows for precise measurements of the fluxes. Furthermore, these detectors have a very good energy resolution for deposited energy measurements. The study of deposited energy in semiconductors is interesting to validate the models used to calculate the radiation effects on microelectronics components. Finally, thanks to discrimination in pulse height and pulse shape, we can distinguish the primary direct ionization component from the impurities of the beam.

2. Experimental setup

2.1. Irradiation setup

The measurements were carried out in the H8 beamline of the CERN SPS North experimental Area (SPS-NA), which is described in detail in Refs. [4,10]. The 150 GeV/nucleon SPS Pb beam arrives in 10 s long spills, with an intensity varying between 10^3 and 10^5 ions/spill (the intensity can be easily tuned for different runs). The beam size was set
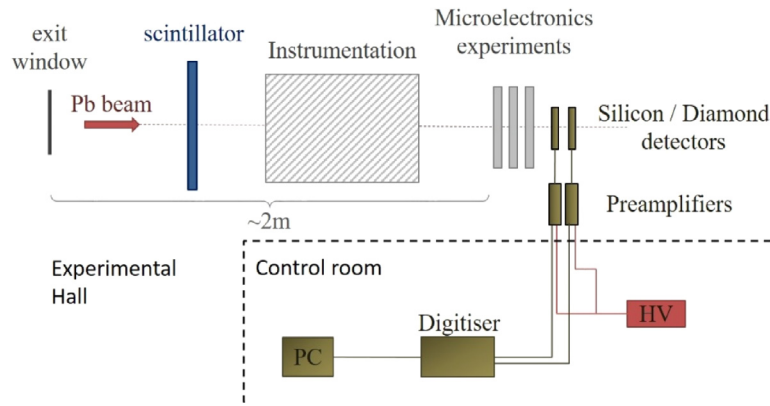
Fig. 1. Schematics of the experimental Setup to measure with silicon and diamond detectors at the H8 beamline of the CERN SPS North experimental Area.

at approximately 3×3 cm^2 FWHM, therefore larger than the surface of the two detectors, which guaranteed their homogeneous irradiation.

A schematics of the experimental setup is shown in Fig. 1. Multiple experiments are run in parallel to take advantage of the penetration of this beam. Following the exit window of the beam pipe, the instrumentation used to characterize the particle beam was installed. This comprised of a scintillator and a multi wire proportional chamber, which are followed by a scintillating fibre monitor. The experimental test bench is located 0.5 m downstream the latter and approximately 2 m downstream the beam pipe window. On the test bench, a support guarantees that boards and detectors that are tested in parallel remain aligned. The silicon and diamond detectors were mounted on the fourth position of the support to the downstream, following three PCB boards on plexiglass plates. The relatively large amount of material between the beam pipe exit window and the two detectors results in a high beam intensity attenuation and fragmentation of the beam at this rear position, which is examined in detail in [10].

In all experimental cases, at least one of the boards installed in front of the examined detectors is an ESA Single Event Upset monitor [11], a radiation hardened 16 Mbit SRAM module which consist of 4 dies covering a surface of approximately 2×2 cm^2. A control software allows to write and read its dies, count the generated errors during and post-irradiation and display their physical arrangement in the memory [12]. Therefore, the ESA SEU monitor was used to guarantee the good alignment of the beam with the silicon and the diamond detector.

2.2. Detectors

Two solid-state detectors were tested in the SPS-NA, a silicon diode detector by Micron Semiconductors Ltd. [13] and a single crystal diamond detector grown by chemical vapour deposition by Element Six [14]. The silicon detector comprises a square (2 mm × 2 mm × 140 µm) totally depleted p–n junction diode, a ceramic PCB and housing of aluminium. The diamond detector is also square (2 mm × 2 mm × 300 µm), has a metallic contact area of 1.5 mm × 1.5 mm.

The detectors are operated in pulse mode. Both detectors are connected to a low-noise current amplifier (Cividec C1 [15]), which is characterized by a 2 GHz analog bandwidth and a 20 dB gain.

The signals are fed to a digitizer, 10 bits, 1 Gsample/s, DT5751 by CAEN [16]. Each waveform above threshold is saved and the processing analysis is done offline.

This electronics chain was chosen to have fast signals and minimal shaping introduced. The silicon detector is reversed biased with +40 V, the diamond is biased with +240 V.

A logic signal from the accelerator is also recorded to give the start time of a spill extraction. This can be used to associate each waveform to the respective spill using the timestamp information.
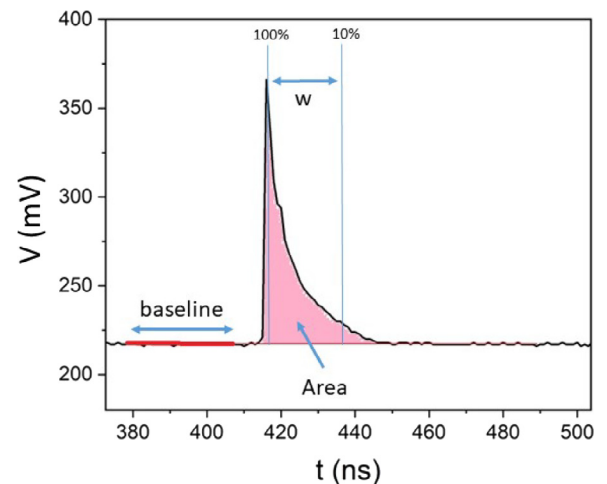

Fig. 2. Example of a measured waveform for illustration of the data analysis.

3. Waveform analysis

The raw data of all waveforms, voltage as a function of time V(t), are analysed offline and Fig. 2 represents a graphic example of the analysis. The signal baseline is measured by averaging 20 points on the signal pre-trigger. We can notice that the signal are very fast, with a rise time of a few ns and a fall time in the order of 10 s of ns.

The deposited energy (E_{dep}) is measured for each recorded waveform by integrating the voltage signal in time V(t) (i.e. measuring the area of the signal). The method has been also presented in Ref. [17]. E_{dep} is proportional to the charge produced by the ionization and to the energy necessary for pair production E_{eh} (3.67 eV for silicon and 13 eV for diamond).

$$E_{dep} = \frac{E_{eh}}{e \cdot G} \cdot \int \frac{V(t)}{R} dt$$

where G is the Gain of the preamplifier (20 dB as calibrated by the manufacturer), R is 50 Ω and e is the elementary charge.

The deposited energy spectra can therefore be built and are presented in Fig. 3 for the two detectors. For both a well-defined peak is present, which is due to the direct ionization of ultra-high energy lead ions passing through the detector. The deposited energy is discussed in a later section in comparison to simulations. A continuum is present at lower deposited energy in the spectrum with an intensity of about an order of magnitude less with respect to the peak. The best interpretation is that these events are due to fragments and impurities present in the beam at that position.
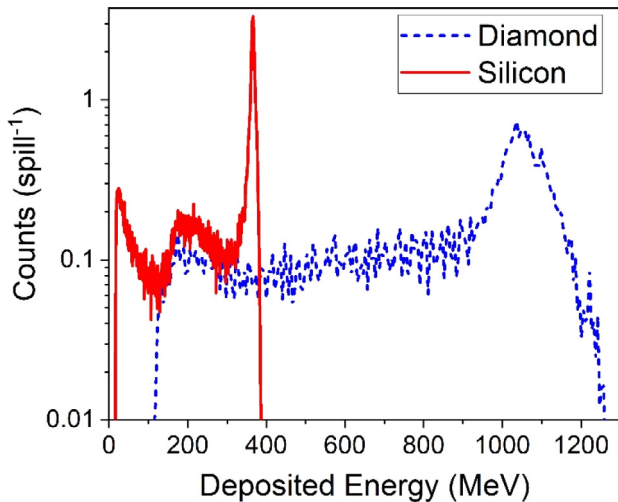
Fig. 3. Deposited energy spectra of an ultra-high energy lead ion beam measured with a silicon and a diamond detector.

The use of a fast electronic chain and digitalization of the signal allows for a study of Pulse Shape Discrimination (PSD). It is well known that in solid state detectors the shape of the signal depends on the density and geometry of the charge deposition [18]. It has been shown in nuclear physics experiments that this method can successfully discriminate reaction products and be a complementary method to the more established $\Delta E - E$ and time of flight techniques [19–23].

The PSD is based on a bi-parametric analysis, where the first parameter is the deposited energy, and the second parameter defined on the shape of the signal. Using a current preamplifier, the signal shaping is minimal, and a natural choice of the parameter is the fall time of the signal [24]. If a more traditional charge preamplifier were used, which integrates the signal, the natural choice would have been the rise time [18,25]. Sometimes the second moment value of the signal is also used [26]. We choose to use the fall time of a signal (w) defined as the time from 100% to 10% of the signal (see Fig. 2). Fig. 4 shows the results of the bi-parametric analysis plotted as a density distribution. The projection on the fall time axis is shown as a histogram in Fig. 5.

Looking at the distributions of Figs. 4 and 5, it is found that the signals can be divided in different regions of interest. For the case of the silicon, we define four regions of interest (see Fig. 5): a plateau at low fall time, a peak, a second plateau and finally a broader peak. For the case of the diamond, we define only two regions of interest: a first peak at low fall time and a continuum for higher fall time.

Fig. 6 shows examples of a signal randomly selected for each of the four regions of interest. It is clear that they have a different shape that can also be qualitatively appreciated by looking at the graphics.

The observation that pulse shape discrimination is more difficult with a diamond detector must be explained by the higher mobility of charge carrier, which makes diamond signals faster. In fact, diamond does look like a compressed (in time) version of the Silicon. Possibly better discrimination can be achieved with a digitizer with higher sampling rate. This is a possible development for future tests.

The projection on the deposited energy axis of the distributions shown in Fig. 4 is of course represented by Fig. 3. Fig. 7 reproduces the same projection adding constrains of the region of interests identified in Fig. 5.

4. Beam diagnostics results

The analysis presented in the previous section can be used for beam diagnostics that will be useful to scientists using the beam for
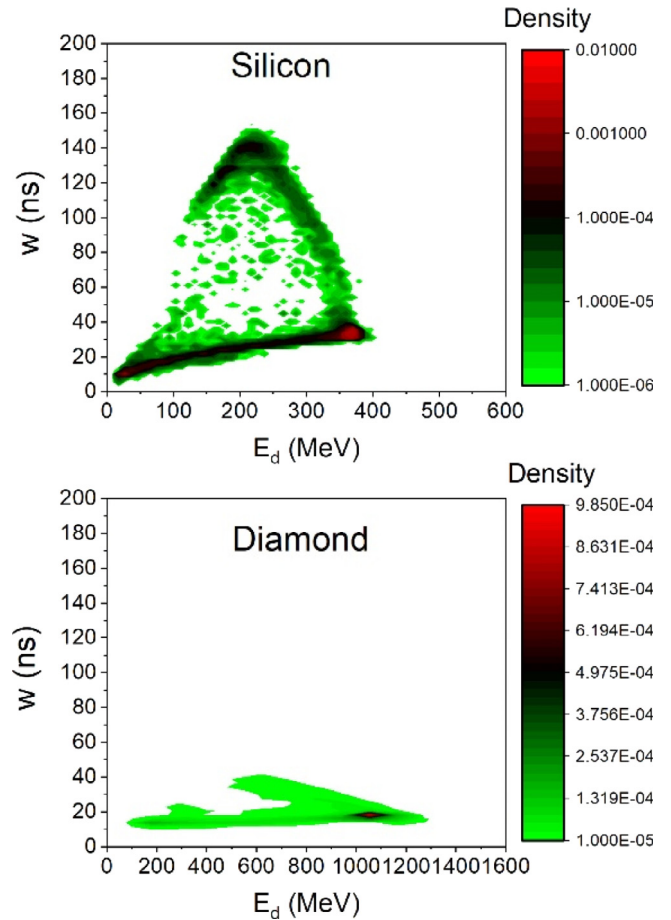

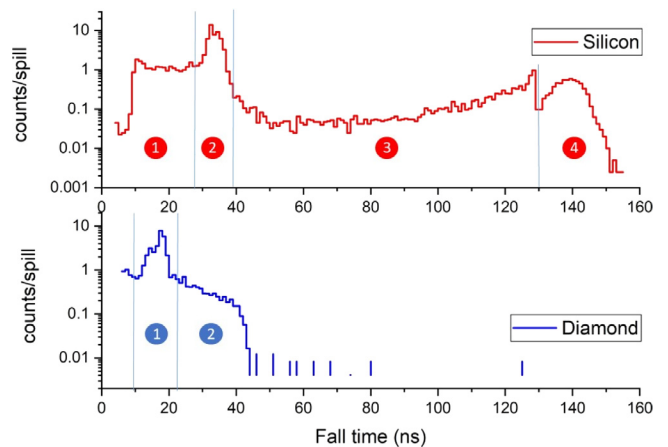**Fig. 4.** Bi-parametric analysis of silicon and diamond events.

Fig. 5. Fall time distribution of the signals measured for silicon and diamond detectors. The vertical lines represent the limits defined for the data analysis and numbers are labels of the defined regions.

irradiation. The first information that can be useful is the beam composition at the detector position. We are interested to discriminate the primary component of 150 GeV/nucleon lead ions and the impurity components. The direct component can be completely discriminated by PSD on silicon (type 2 signals in silicon), while for diamond we also apply a threshold in energy deposition (type 1 signals in diamond and with $E_d > 900$ MeV). The energy deposition threshold value $E_d > 900$ MeV is chosen to cut just under the main peak.
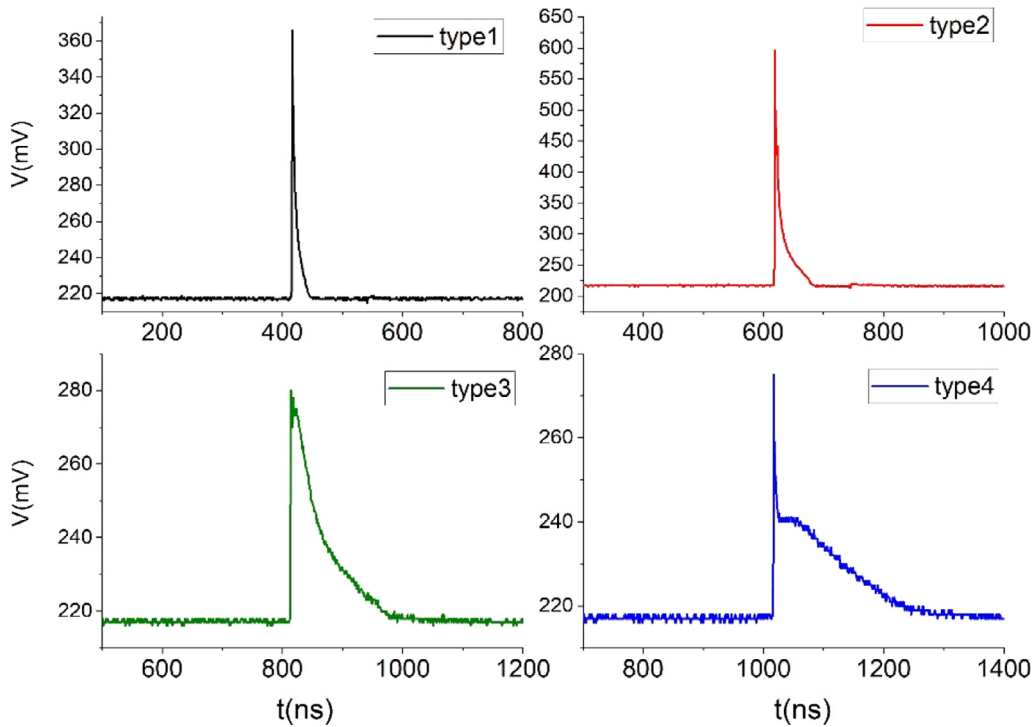
Fig. 6. Examples of signals measured with a silicon detector and selected in the four region of interest of the fall time distribution (Fig. 5).
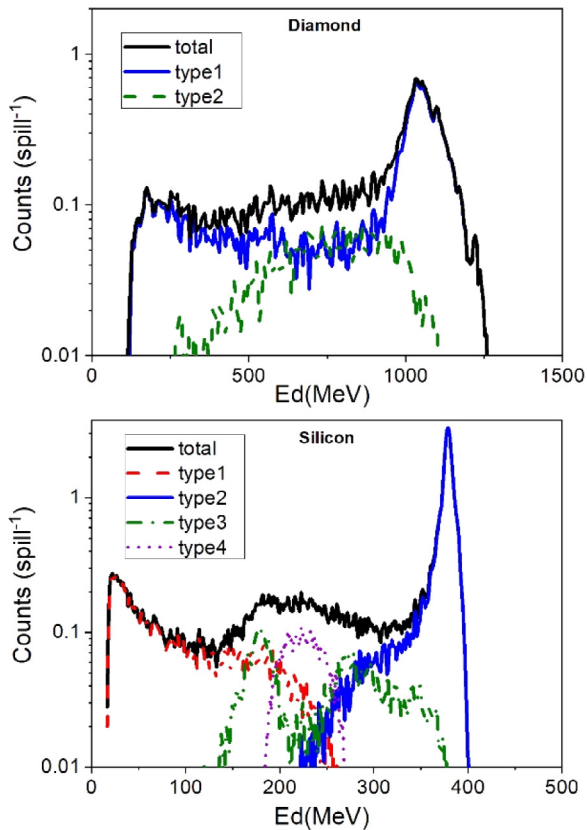

Fig. 7. Deposited energy spectra of an ultra-high energy lead ion beam measured with a silicon and a diamond detector. Spectra have been built using PSD.

Both for the Silicon and Diamond detector, the best interpretation is that signals with larger fall time (type 3 and 4 in silicon and type 2 in diamond) are heavy ions (fission fragments) with high energy. A later discussion adds justification to this interpretation.

Signals with short fall time below the full peak (type 1 for silicon, type 1 and with $E_d < 900$ MeV), are lighter or faster fragments with lower LET that are punching through the detector.

Using these criteria, Fig. 8 shows the results for the beam composition according to the Silicon and Diamond detectors. It is encouraging that the two detectors are in good agreement, showing a direct component of about 55% with respect to the total number of events. The high fraction of fragments is not unexpected, as the detectors were tested in a rear position with many other experiments and materials in front. This also shows the increasing importance of local diagnostics measurements when the beam is highly fragmented.

Fig. 9 shows the measured time structure of the beam spills. This is built using the time difference between every event and the extraction signal from the accelerator. The knowledge of this structure can be important for those applications that are limited by flux, e.g. that suffer from dead time. In fact if the accelerator is not continuous one needs to keep into account that the flux is not constant, but modulated by this spill structure.

Fig. 10 shows a time trace of the flux measured by the silicon detector. This shows that even with a small 2×2 mm^2 detector there is enough statistics to monitor the evolution of the beam. In this particular run we observe that the intensity of the beam had been deliberately modulated by the operators, alternating high flux periods to short off periods.

5. Discussion

5.1. Deposited energy and simulations

Monte Carlo simulation of radiation transport can be an important tool for data interpretation. In this work we used both FLUKA and GEANT4 for comparison. The first interesting observation is about the deposited energy of the primary lead ion beam. For silicon, this gives a peak in the spectrum at about $E_{dep} = 350$ MeV. Simulations confirm that this peak is indeed due to the primary beam that goes through the detector. We can see that both simulations of deposited energy are in agreement within 15%. For silicon, Geant4 simulations seem to have a
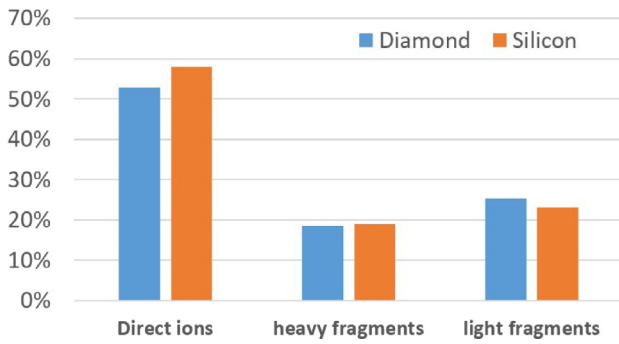
Fig. 8. Beam composition measured using silicon and diamond detectors with pulse height and PSD. Direct ions are ultra-high energy lead ions (150 GeV/nucleon).
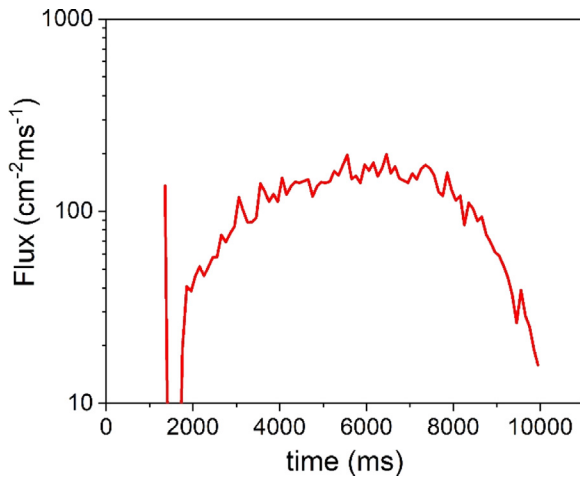

Fig. 9. Average time profile of a spill of ultra-high energy lead ions measured with a silicon detector.
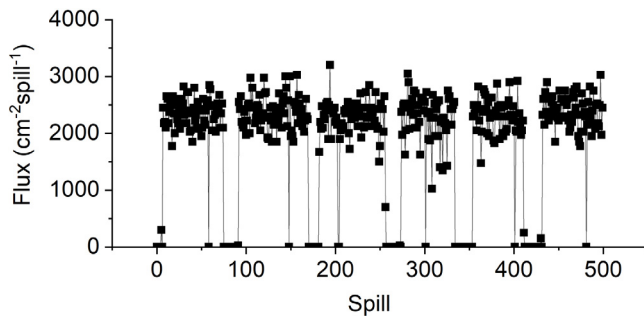

Fig. 10. Time trace of the ions flux, spill by spill, measured with a silicon detector.

better agreement (within 3%), while for diamond FLUKA simulations are closer. However comments should be made: (A) the measured deposited energy is dependent on the calibration of the gain of the preamplifier, and it is reasonable to expect a systematic error. Also, the gain is assumed to be constant, but one can expect some degree of non-linearity when extrapolating to different order of magnitudes. (B) The simulations will use different models and algorithms to transport the radiation, and these models become more uncertain at these energy ranges. Something important to consider is for example how δ-rays are treated, as discussed in Ref. [27]. The discussion of these details goes outside the scope of this paper, but it is important to notice that benchmarking of simulations is important as they are used also to develop models for the interpretation and prediction of SEE in microelectronics [28,29]. (C) Possibly an import source of uncertainty
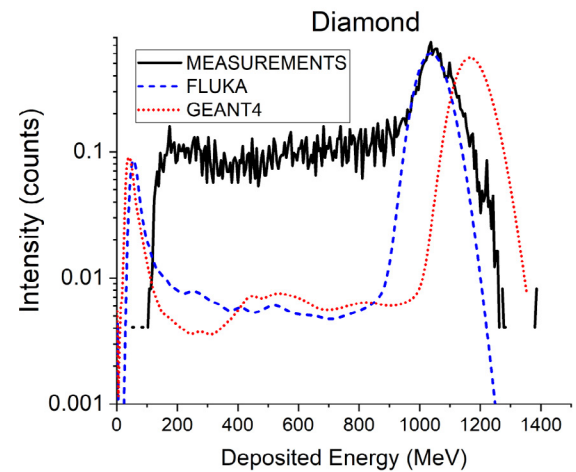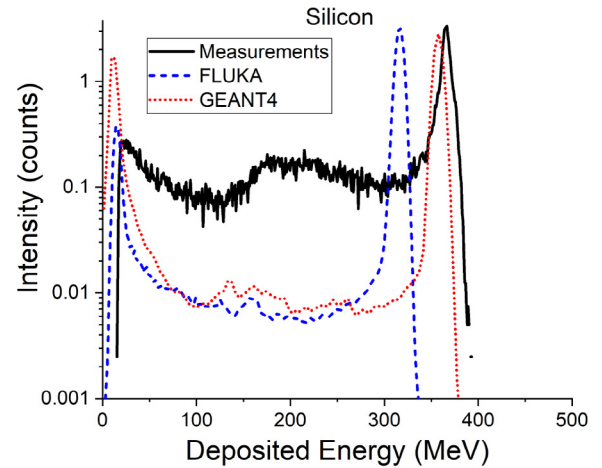

Fig. 11. Deposited energy spectrum compared to Monte Carlo simulations for silicon (top) and diamond (bottom). Monte Carlo simulations are performed with GEANT4 and FLUKA and results have been convoluted with the measured resolution.

is the missing knowledge of the materials in front of the detector in the beam. Although this is clearly not independent for the two detectors and it should produce a similar uncertainty.

5.2. Beam fragmentation and impurities

The fragmentation of 158 GeV/nucleon Lead ions has been studied at CERN by dedicated experiments [30,31]. In these reference a cross section σ of fragmentation has been reported for Silicon and Carbon to be 3.5 b and 3.1 b, respectively. Using the following formula, we can give a back of the envelope calculation of the fraction of fragmentation respect to the primary beam that occur in the detector volume, where I_0 is the intensity of the primary beam before interaction, ρ is the material density, M is the molar mass, N_{av} is Avogadro number, and x is the thickness of the material.

$$\frac{I_0 - I}{I_0} = 1 - \exp\left[-\sigma \cdot \frac{\rho}{M} N_{av} \cdot x\right]$$

Using the correct values, we find that fragmentation is 0.25% in the silicon detector and 1.5% in the diamond detector. This calculation has been confirmed by Monte Carlo calculations, where we find that fragmentation in the detectors is 0.58% and 1.2%, respectively. This suggests that most of the fragments that we observed are produced by all the other materials that are in the beamline in front of our detectors.

Since it was not possible to know the exact geometry of the other experiments and what materials where in the beam path, we tried,

as an example, to run simulations with 5 mm of Al in front of the detector (at 5 cm distance). Here the fragmentation rises to about 9%, confirming that most of the impurities are not produced in the detectors themselves. However, as we can also see in Fig. 11, we are still far from the levels that are measured in the order of 40%.

Considering this fragment fraction, we shall also exclude the possibility that this effect is due to a partial collection of the charge carriers. Firstly, it would be very improbable to see such a similar effect in two detectors with a very different geometry, material and construction. Secondly, both detectors behave well when calibrated with mono-energetic alpha particles, such that the full energy peak is neat, without structures due to partial collection.

It is also interesting to notice that we can simulate what ions are produced by the nuclear reactions. In Fig. 12 we report a distribution of the produced ions in mass A and atomic number Z for the case of 5 mm aluminium separated by 5 mm air for the 140 μm silicon detector and the 300 μm diamond detector. Here the ions are scored in the detector volume.

As a future development of the simulations, we can try to change the materials that are in front of the detector. Also, we are looking forward to repeat an experimental campaign in order to try the detectors in multiple positions, including a front position where the direct component would be much higher.

5.3. Pulse shape analysis

More discussion is needed to justify the interpretation of the pulse shape analysis and in particular the capability of particle separation. It has to be noticed that this technique is usually performed for nuclear physics experiments where energy ranges are in the order of 10 s MeV/nucleon, complex multi-detector systems are used, and it is often combined with other techniques, like time of flight and $\Delta E - E$ [20–22]. In those systems good resolutions in particle separation can be achieved. In this work, we extrapolate this technique to ultra-high energies, 150 GeV/nucleon, which is a first to the best of our knowledge. Also, the detectors are designed as beam monitors, presenting a very fast electronic chain, that is optimal for in-beam measurements, but certainly not optimal for resolution.

The interpretation for particle separation is based on the fact that the signal shape becomes very sensitive to the density and length of the ionization track [18]. The reason is the plasma effect [32] and the finite drift time of charge carriers, electron and holes [33]. As a result, if the incident energy is kept constant, the charge-collection time, and therefore the fall time, increases monotonously with charge Z and mass number A of the detected ion [34]. If Z and A are kept constant, the dependence on the particle energy is more complex, but for incident ions with long ranges in silicon the charge-collection time increases with the square root of dE/dx [34].

6. Conclusions

It has been shown that silicon and diamond detectors with a fast readout electronics chain can be used for the diagnostics of ultra-high energy ion beams such the ones produced by the SPS accelerator at CERN.

Tests with 150 GeV/nucleon lead ions show that the detectors can discriminate the direct component of the beam from fragment impurities. This is particularly important in the case of using such beams for testing of microelectronics, as experiments are running in parallel one behind the other to maximize the use of the beam, and position sensitive diagnostics is favoured by the small size of the detectors.

The discrimination was possible thanks to a combination of deposited energy and pulse shape analysis. Comparing the two detectors, we can say that the silicon offers the best discrimination capability, but the diamond can always be preferred in case of high flux application, being more radiation hard, and we show that comparable results are possible.
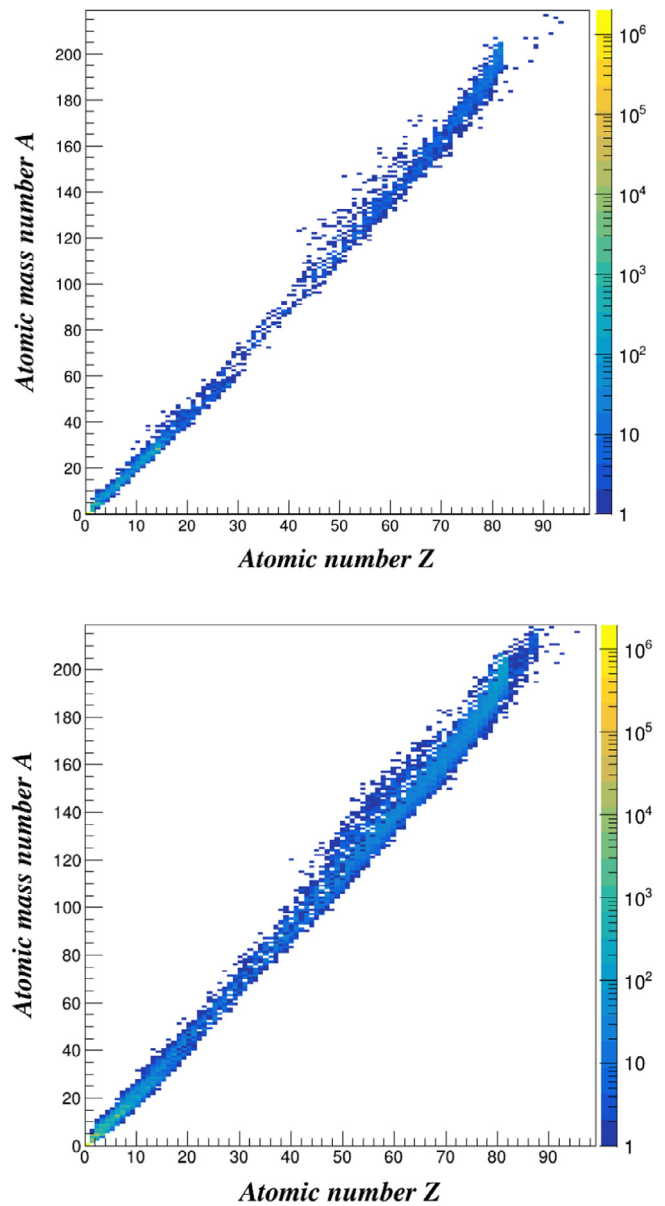

Fig. 12. Distribution of the produced ions as a function of Z and A simulated with GEANT4 for the silicon detector (top) and diamond detector (bottom).

Declaration of competing interest

The authors declare that they have no known competing financial interests or personal relationships that could have appeared to influence the work reported in this paper.

References

[1] Bastiaan de Raad, The CERN SPS proton–antiproton collider, IEEE Trans. Nucl. Sci. 32 (5) (1985) 1650–1652.

[2] M.C. Abreu, et al., Evidence for deconfinement of quarks and gluons from the J/ψ suppression pattern measured in Pb-Pb collisions at the CERN-SPS, Phys. Lett. B 477 (1–3) (2000) 28–36.

[3] N. Abgrall, et al., NA61/SHINE Facility at the CERN SPS: beams and detector system, J. Instrum. 9 (06) (2014) P06005.

[4] R. Garcia Alia, et al., Ultra-energetic heavy ion beams in the CERN accelerator complex for radiation effects testing, IEEE Trans. Nucl. Sci. 66 (1) (2019) 458–465.

[5] Paul E. Dodd, Physics-based simulation of single-event effects, IEEE Trans. Device Mater. Reliab. 5 (3) (2005) 343–357.

[6] James C. Pickel, Single-event effects rate prediction, IEEE Trans. Nucl. Sci. 43 (2) (1996) 483–495.

[7] Robert A. Reed, et al., Single-event effects ground testing and on-orbit rate prediction methods: the past, present, and future, IEEE Trans. Nucl. Sci. 50 (3) (2003) 622–634.

[8] F. Trom, Tetsuo F. Miyahira, Test results of single-event effects conducted by the jet propulsion laboratory, in: IEEE Radiation Effects Data Workshop, IEEE, 2005.

[9] Rubén García Alía, et al., Single event effects in high-energy accelerators, Semicond. Sci. Technol. 32 (3) (2017) 034003.

[10] Maria Kastriotou, et al., Single event effect testing with ultra-high energy heavy ion beams, IEEE Trans. Nucl. Sci. (2019).

[11] R. Harboe-Sorensen, et al., PROBA-II Technology demonstration module in-flight data analysis, IEEE Trans. Nucl. Sci. 59 (4) (2012) 1086–1091.

[12] P. Fernandez Martinez, et al., SEE Tests with ultra energetic Xe ion beam in the CHARM facility at CERN, IEEE Trans. Nucl. Sci. 66 (2019) 1523–1531, http://dx.doi.org/10.1109/TNS.2019.2907112.

[13] Micron semiconductors, http://www.micronsemiconductor.co.uk/silicon-detector-catalogue/.

[14] Element six, https://www.e6.com/en/.

[15] Cividec, https://cividec.at/.

[16] CAEN, https://www.caen.it/.

[17] Carlo Cazzaniga, et al., Study of the deposited energy spectra in silicon by high energy neutron and mixed fields, IEEE Trans. Nucl. Sci. (2019).

[18] G. Pausch, et al., Identification of light charged particles and heavy ions in silicon detectors by means of pulse-shape discrimination, in: 1995 IEEE Nuclear Science Symposium and Medical Imaging Conference Record, vol. 1, IEEE, 1995.

[19] K. Mahata, et al., Particle identification using digital pulse shape discrimination in a nTD silicon detector with a 1 GHz sampling digitizer, Nucl. Instrum. Phys. Res. A 894 (2018) 20–24.

[20] L. Bardelli, et al., Progresses in the pulse shape identification with silicon detectors within the FAZIA collaboration, Nucl. Instrum. Methods Phys. Res. A 654 (1) (2011) 272–278.

[21] S. Carboni, et al., Particle identification using the ΔE–E technique and pulse shape discrimination with the silicon detectors of the FAZIA project, Nucl. Instrum. Methods Phys. Res. A 664 (1) (2012) 251–263.

[22] D. Beaumel, GASPARD collaboration, The GASPARD project, Nucl. Instrum. Methods Phys. Res. B 317 (2013) 661–663.

[23] M. Alderighi, et al., Charge identification in large area planar silicon detectors, using digital pulse shape acquisition, IEEE Trans. Nucl. Sci. 53 (1) (2006) 279–285.

[24] S. Barlini, et al., New digital techniques applied to A and Z identification using pulse shape discrimination of silicon detector current signals, Nucl. Instrum. Methods Phys. Res. A 600 (3) (2009) 644–650.

[25] M. Mutterer, et al., Breakthrough in pulse-shape based particle identification with silicon detectors, in: 1999 IEEE Nuclear Science Symposium. Conference Record. 1999 Nuclear Science Symposium and Medical Imaging Conference (Cat. No. 99CH37019), vol. 1, IEEE, 1999.

[26] H. Hamrita, et al., Charge and current-sensitive preamplifiers for pulse shape discrimination techniques with silicon detectors, Nucl. Instrum. Methods Phys. Res. A 531 (3) (2004) 607–615.

[27] Vanessa Wyrwoll, et al., Longitudinal direct ionization impact of heavy ions on SEE testing for ultra-high energies, IEEE Trans. Nucl. Sci. (2020).

[28] Vanessa Wyrwoll, et al., Heavy ion nuclear reaction impact on SEE testing: from standard to ultra-high energies, IEEE Trans. Nucl. Sci. (2020).

[29] M. Bagatin, et al., Characterizing high-energy ion beams with PIPS detectors, IEEE Trans. Nucl. Sci. (2019).

[30] V. Togo, et al., Fragmentation studies of high-energy ions using CR39 nuclear track detectors, Nucl. Instrum. Methods Phys. Res. A 580 (1) (2007) 58–61.

[31] M. Giorgini, S. Manzoor, Fragmentation of very high energy heavy ions, Nucleus–Nucleus Collisions 1 (2001) 149–152.

[32] W. Seibt, Karl-Erik Sundström, P.A. Tove, Charge collection in silicon detectors for strongly ionizing particles, Nucl. Instrum. Methods 113 (3) (1973) 317–324.

[33] C.A.J. Ammerlaan, R.F. Rumphorst, L.A.Ch. Koerts, Particle identification by pulse shape discrimination in the pin type semiconductor detector, Nucl. Instrum. Methods 22 (1963) 189–200.

[34] J.B.A. England, G.M. Field, T.R. Ophel, Z-identification of charged particles by signal risetime in silicon surface barrier detectors, Nucl. Instrum. Methods Phys. Res. A 280 (2–3) (1989) 291–298.